Colours of black holes: infrared flares from the hot accretion disc in XTE J1550–564

Juri Poutanen,[1,2]★ Alexandra Veledina[1,2] and Mikhail G. Revnivtsev[3]

[1]*Tuorla Observatory, Department of Physics and Astronomy, University of Turku, Väisäläntie 20, FI-21500 Piikkiö, Finland*
[2]*Astronomy Division, Department of Physics, PO Box 3000, FI-90014 University of Oulu, Finland*
[3]*Space Research Institute, Russian Academy of Sciences, Profsoyuznaya 84/32, 117997 Moscow, Russia*

ABSTRACT

Outbursts of the black hole (BH) X-ray binaries are dramatic events occurring in our Galaxy approximately once a year. They are detected by the X-ray telescopes and often monitored at longer wavelengths. We analyse the X-ray and optical/infrared (OIR) light curves of the BH binary XTE J1550–564 during the 2000 outburst. By using the observed extreme colours as well as the characteristic decay time-scales of the OIR and X-ray light curves, we put strong constraints on the extinction towards the source. We accurately separate the contributions to the OIR flux of the irradiated accretion disc and a non-thermal component. We show that the OIR non-thermal component appears during the X-ray state transitions both during the rising and the decaying part of the outburst at nearly the same X-ray hardness but at luminosities differing by a factor of 3. The line marking the quenching/recovery of the non-thermal component at the X-ray hardness–flux diagram seems to coincide with the 'jet line' that marks the presence of the compact radio jet. The inferred spectral shape and the evolution of the non-thermal component during the outburst, however, are not consistent with the jet origin, but are naturally explained in terms of the hybrid hot flow scenario, where non-thermal electrons emit synchrotron radiation in the OIR band. This implies a close, possibly causal connection between the presence of the hot flow and the compact jet. We find that the non-thermal component is hardening during the hard state at the decaying stage of the outburst, which indicates that the acceleration efficiency is a steep function of radius at low accretion rate.

Key words: accretion, accretion discs – black hole physics – radiation mechanisms: non-thermal – X-rays: binaries.

1 INTRODUCTION

The optical/infrared (OIR) spectra of black hole (BH) low-mass X-ray binaries often show an excess above the standard (Shakura & Sunyaev 1973) accretion disc emission (e.g. Hynes et al. 2000, 2002; Gelino, Gelino & Harrison 2010). In some cases, the spectrum can be described by a power law of index close to zero (i.e. $F_\nu \propto \nu^0$). There are three possible candidates that may account for this emission: the irradiated disc (Cunningham 1976; Gierliński, Done & Page 2009), hot accretion flow (Veledina, Poutanen & Vurm 2013a) and the jet (Hynes et al. 2002; Gallo et al. 2007). Sometimes the OIR fluxes are higher than expected from any candidate alone (Chaty et al. 2003; Gandhi et al. 2010), and the complex optical/X-ray cross-correlation functions (Kanbach et al. 2001; Durant et al. 2008) support this anticipation, suggesting contribution

of two components simultaneously (Veledina, Poutanen & Vurm 2011b). The source of OIR emission cannot be determined by only using photometric data and some additional information about the OIR–X-ray connection, short time-scale variability properties and the long-term spectral variations is required (see review in Poutanen & Veledina 2014). The latter is particularly important when trying to separate emission of different components.

The entire transition of the BH transient XTE J1550–564 from the hard to the soft state and back during its 2000 outburst was monitored by Yale 1 m telescope at CTIO in the *V*, *I* and *H* filters (Jain et al. 2001b). The light-curve structure cannot be simply explained by the fast rise-exponential decay pattern, expected in the case of standard or irradiated disc. An additional component, manifesting itself through strong flares, is required. Recently, Russell et al. (2010, 2011) suggested that this component originates in a radio-emitting jet; however, multiple errors in these works make this interpretation doubtful. Here, we re-analyse the available OIR and X-ray data. From the characteristic decay time-scales in the

★ E-mail: juri.poutanen@utu.fi
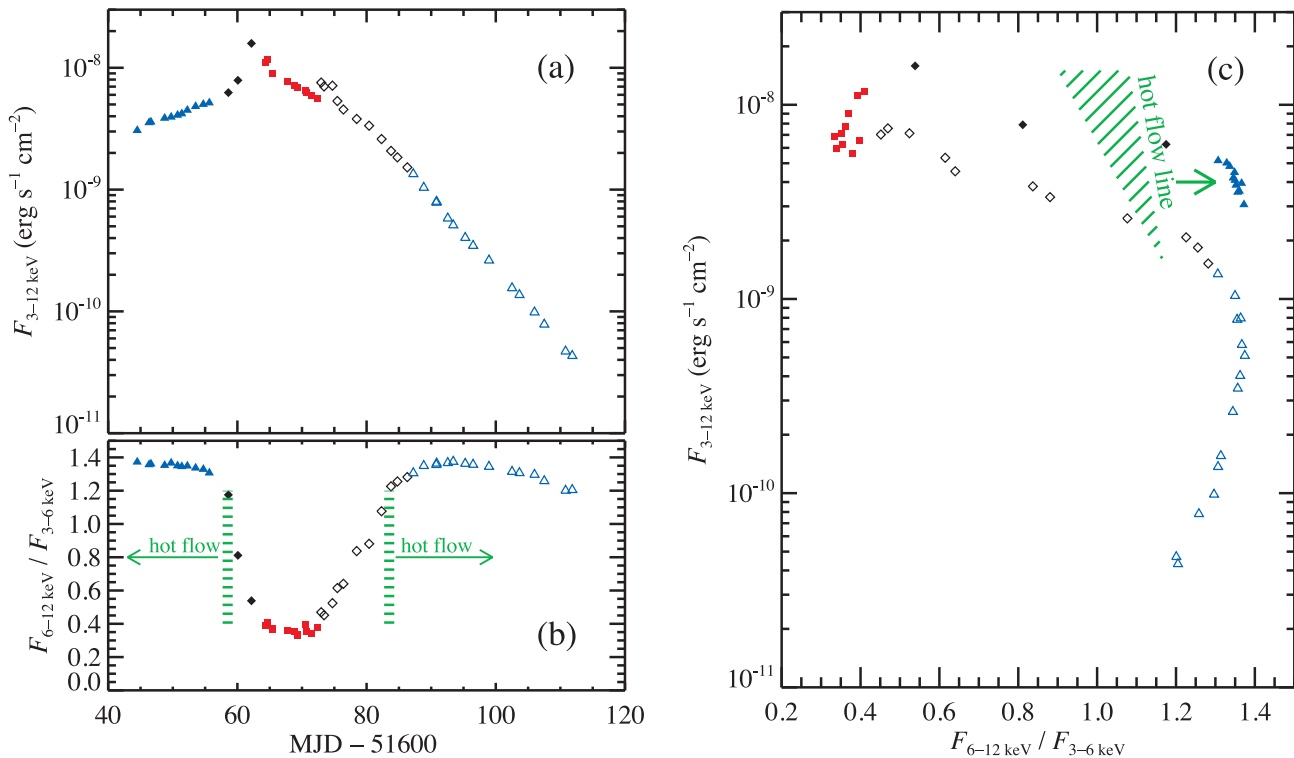
Figure 1. (a) Light curve of XTE J1550–564 (flux in the 3–12 keV band) and (b) the evolution of the hardness ratio (i.e. ratio of fluxes in the energy bands 6–12 and 3–6 keV) during the 2000 outburst. (c) The hardness–flux diagram. Different symbols and colours highlight outburst stages defined from the hardness ratio (see text). The times and the positions of quenching/recovery of the non-thermal OIR component ('hot flow line') are marked by green ribbons.

X-rays and in different OIR filters, we infer the typical accretion disc temperature during the soft state. This immediately translates to the constraints on the extinction towards the source, poorly known before. Using the OIR light curves, we accurately extract the non-disc non-thermal component and show evolution of its spectral shape during the flare. We find that the additional component may originate in the hot accretion flow, if a small fraction of energy is injected in the form of non-thermal electrons that emit synchrotron radiation.

2 LIGHT CURVES AND EXTINCTION

2.1 Data

The X-ray data on the 2000 outburst of XTE J1550–564 covering 2.5–25 keV range from the Proportional Counter Array (PCA) spectrometer (Jahoda et al. 2006) on board the *Rossi X-ray Timing Explorer (RXTE)* were analysed with the HEASOFT package (version 6.15) and response matrices were generated using PCARSP (11.7.1). The instrumental background of the PCA detectors was estimated with CM_bright_VLE model. At the position of the source XTE J1550–564 there is additional sky background from the so-called Galactic ridge (see Revnivtsev et al. 2006, and references therein), which provides the flux at the level of $F_{3–20\,keV} \sim 1.2 \times 10^{-11}$ erg s^{-1} cm^{-2} within field of view of PCA ($\sim$1 deg^2). In order to account for this additional background, we have used *RXTE*/PCA observations of XTE J1550–564 in 2001 April when the source was already in quiescence. All the spectral data were fitted using XSPEC 12.8.1g package (Arnaud 1996), assuming 1 per cent systematic uncertainty. To estimate fluxes from the source, we have fitted the spectral data with a standard for

BHs DISKBB+POWERLAW model and corrected the model fluxes in the specific energy bands by the ratio of the data to the model. For a more detailed spectral modelling, we also fitted the data with a hybrid Comptonization model COMPPS (Poutanen & Svensson 1996) and a cutoff power-law model with Compton reflection PEXRAV (Magdziarz & Zdziarski 1995). Interstellar absorption was taken into account using WABS model with the neutral hydrogen column density of $N_{\mathrm{H}} = 0.80 \times 10^{22}$ cm^{-2} (Miller et al. 2003).

The X-ray light curve is shown in Fig. 1 together with the evolution of the hardness ratio as well as with the hardness–flux diagram. It is coloured according to the hardness ratio. The hard state is shown by blue triangles, while the transitions from the hard to the soft state and back are shown by black diamonds. The filled and open symbols correspond to the rising and decaying phases of the outburst, respectively. The soft state with the nearly constant hardness ratio is shown by red squares.

The OIR data from the 2000 outburst in *V*, *I* and *H* filters have been presented by Jain et al. (2001b). To convert magnitudes to fluxes, we use the zero-points of 3636, 2416 and 1021 Jy and the effective wavelengths of 545, 798 and 1630 nm for filters *V*, *I* and *H*, respectively (Bessell, Castelli & Plez 1998). We show the daily-averaged OIR light curves in Fig. 2. The colour code is the same as in Fig. 1, with additional magenta points corresponding to the quiescent state of the source. The fast rise-exponential decay morphology is accompanied here with flares, which are most prominent in the *H* filter.

2.2 Soft state and implications for the disc temperature

During the soft (and the following intermediate) state, the OIR emission is likely originating in the irradiated accretion disc alone. This
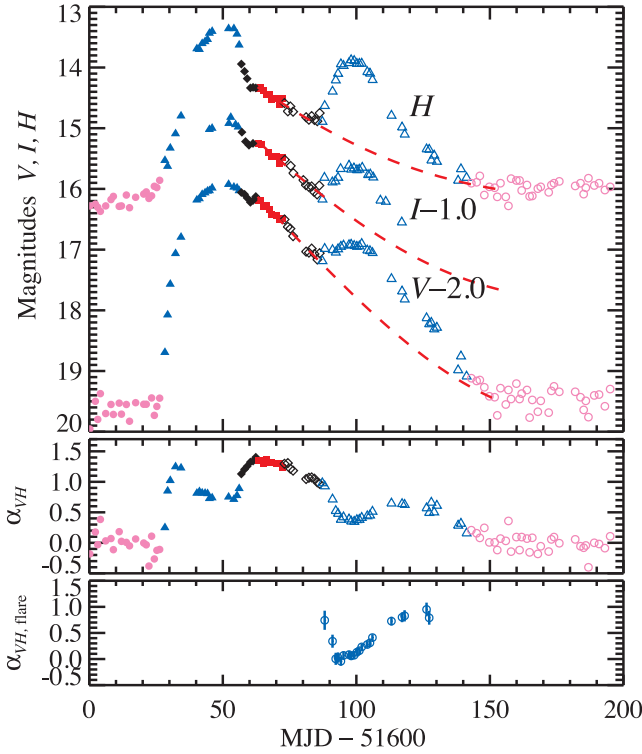
Figure 2. Light curve of XTE J1550–564 in three filters *V*, *I* and *H* during the 2000 outburst. The *V* and *I* magnitudes are shifted upwards by 2.0 and 1.0, respectively. Pink symbols correspond to the quiescent state, other symbols are the same as in Fig. 1. The red dashed lines show the evolution of the irradiated disc during the second flare (see Section 3.4). The middle panel show the power-law spectral index of the intrinsic spectrum α_{VH} corrected for extinction (with $A_V = 5.0$) determined from the $V-H$ colour using equation (9). The lower panel shows the evolution of the spectral index of the flare component.

Table 1. Parameters of the system adopted from Orosz et al. (2011).

Orbital period	$P_{\rm orb}$	37 h
Distance	D	4.38 kpc
Black hole mass	M_1	9.1 $M_\odot$
Companion mass	M_2	0.3 $M_\odot$
Inclination	i	75°
Separation	a	11.85 $R_\odot$
Radius of the companion	R_2	1.75 $R_\odot$
Roche lobe size	$R_{L,1}$	7.7 $R_\odot$
Effective temperature of the companion	$T_{\rm eff}$	4475 K

is supported by a simple exponential shape of the light curves in both the OIR and X-ray bands. This knowledge can be used to estimate the accretion disc temperature. The first constraint relates the peak X-ray luminosity to the reprocessed optical flux. The effective temperature at the outer radius of the irradiated disc dominating the OIR emission is $T_{\rm eff,irr} = [\eta(1 - A)L_{\rm X}/(4\pi R_{\rm irr}^2 \sigma_{\rm SB})]^{1/4}$, where A is the disc albedo and the factor $\eta \approx \frac{H}{R}(\frac{\mathrm{d}\ln H}{\mathrm{d}\ln R} - 1)$ gives the cosine between the normal to the outer disc and the direction to the central X-ray source (Frank, King & Raine 2002). The disc size $R_{\rm irr}$ is a fraction of the Roche lobe (Eggleton 1983, see parameters in Table 1),

$$R_{L,1} = a\frac{0.49q^{2/3}}{0.6q^{2/3} + \ln(1 + q^{1/3})}. \tag{1}$$

For measured $a = 11.85\,{\rm R}_\odot$ and $q = 1/30$, we get $R_{L,1} = 7.7\,{\rm R}_\odot$. The maximum disc size limited by tidal forces is (Warner 1995) $R_{\rm irr} \lesssim 0.6a/(1 + q) \approx 4.8 \times 10^{11}$ cm.

To estimate η, we take the disc half-opening angle of 12° (de Jong, van Paradijs & Augusteijn 1996), i.e. $H/R \sim 0.2$. The logarithmic derivative $\mathrm{d}\ln H/\mathrm{d}\ln R - 1$ takes values 1/8 for the standard and 2/7 for the irradiated discs (Frank et al. 2002), which we adopt in the following and get $\eta \approx 0.06$. A typical albedo A of mostly neutral material is below 0.5 even for a very hard power-law spectrum extending to 100 keV (Basko, Sunyaev & Titarchuk 1974; Magdziarz & Zdziarski 1995) and is expected to be below 0.1 for the blackbody-like X-ray spectra with $kT_{\rm bb} \sim 1.5$ keV in the soft state. The bolometric luminosity at the peak of the 2000 outburst was $\approx 10^{38}$ erg s^{-1} (see Section 3.5). Because only photons with energy above 2 keV thermalize efficiently (Suleimanov, Meyer & Meyer-Hofmeister 1999), we use $L_{>2\,\rm keV} \approx 5 \times 10^{37}$ erg s^{-1} and finally get $T_{\rm eff,irr} \gtrsim 11\,000$ K. The temperature can be lower if the X-rays are so strongly anisotropic that the flux directed towards the outer disc is significantly lower than that at the observed inclination of $i = 75°$. However, if the outer disc is inclined at a similar angle of $\sim80°$ (de Jong et al. 1996), practically no difference is expected.

Further constraints are coming from the comparison of the decay rates in the X-ray and optical bands (Endal, Devinney & Sofia 1976; van Paradijs & McClintock 1995). The general idea is to compare the derivative of the observed flux over temperature to that of the known function – a simple blackbody or the irradiated disc model spectrum. Because the decay rate is an injective (i.e. one-to-one) function of temperature, we immediately obtain the absolute value of $T_{\rm eff}$.

If we ignore energy dissipation intrinsic to the disc (which is possible for high X-ray luminosities), the effective temperature of the irradiated disc varies with the X-ray luminosity as $T_{\rm eff} \propto L_{\rm X}^{1/4}$. Some deviations from this law are possible if the emission pattern is changing. Because the X-ray light curve shows some flares at the transition from the soft to the intermediate state, we have selected the soft-state segment of the data (red squares in Fig. 1) and fitted the X-ray flux there with an exponential profile. We obtain the e-folding time of $\tau_{\rm X} = 10.0 \pm 0.1$ d. This translates to the time of temperature decay $\tau_{\rm T} = 4\tau_{\rm X} = 40$ d, i.e.

$$\partial \ln T_{\rm eff}/\partial t = -1/40\ {\rm d}^{-1}. \tag{2}$$

We then fit the soft- and intermediate-state OIR light curves together with the values in the quiescence at MJD 51645–51650 with a constant plus an exponentially decaying component. For *I* filter, we adopt the constant $I = 19$ in quiescence taken from the earlier observations (Jain et al. 2001a). The e-folding time-scale is then related to the derivative of the logarithm of the flux of the varying (disc) component:

$$\partial \ln F_\lambda/\partial t = -1/\tau_\lambda\ {\rm d}^{-1}. \tag{3}$$

We find $\tau_\lambda = 22.6 \pm 0.8$, 26.0 ± 1.0 and 31.3 ± 2.0 d for the *V*, *I* and *H* bands, respectively. The decay of the blackbody flux due to the decreasing temperature can be computed as

$$\frac{\partial \ln B_\lambda}{\partial \ln T_{\rm eff}} = \frac{y}{1 - \exp(-y)}, \tag{4}$$

where $y = hc/\lambda k T_{\rm eff} = 1.44/(\lambda_\mu T_4)$, λ_μ is the wavelength in microns and $T_4 = 10^{-4}T_{\rm eff}$. The value for the logarithmic derivative is then obtained by dividing equation (3) by equation (2). Solving the resulting equation for $T_{\rm eff}$, we get the average effective soft- and intermediate-state temperatures of 20 800, 19 540 and 17 500 K,

with the errors on individual measurements much smaller than the spread between the values.

We checked the possibility of neglecting the constant flux in the OIR light curves, which resulted in the decay times for the *V*, *I* and *H* bands $\tau_\lambda = 23.8 \pm 0.7$, 29.2 ± 1.1 and 39.2 ± 2.0 d, respectively. These values translate to the temperatures 23 200 and 27 400 K for *V* and *I* filters and for the *H*-filter temperature exceeds 200 000 K. If instead only the soft-state light curve is fitted with the exponential, we get $\tau_\lambda = 29.5 \pm 2.7$, 32.7 ± 3.6 and 41.9 ± 5.4 d, which correspond to $T_{\rm eff}$ in excess of 40 000 K for *V* and *I* filters and no solution is possible for the *H* filter.

We also checked whether the irradiated disc model gives any improvement compared to the simple blackbody. In this case equation (4) can be rewritten as

$$\frac{\partial \ln F_{\rm irr,\lambda}}{\partial \ln T_{\rm out}} = y_{\rm o} \frac{\int_{r_{\rm io}}^1 \frac{\exp(y_{\rm o} x^\beta)}{[\exp(y_{\rm o} x^\beta) - 1]^2} x\,{\rm d}x}{\int_{r_{\rm io}}^1 \frac{x\,{\rm d}x}{\exp(y_{\rm o} x^\beta) - 1}}, \qquad (5)$$

where β is the power-law index of the radial temperature dependence $T(R) \propto R^{-\beta}$, $r_{\rm io} = R_{\rm in}/R_{\rm out}$ is the ratio of the inner to outer disc radius and $y_{\rm o} = hc/\lambda k T_{\rm out}$. In Rayleigh–Jeans regime $y_{\rm o} \ll 1$, the logarithmic derivative takes the minimum value of $(1 - \beta/2)/(1 - \beta)$. We see that for realistic $\beta = 3/7$–$1/2$ (Cunningham 1976; Frank et al. 2002), the model minimum derivatives of 1.4–1.5 are larger than the observed for the *H* filter values $40/\tau_\lambda = 0.95$–1.3, thus no solution is possible. Hence, the simple irradiated disc does not give a good description to the shape of the light curve.

We conclude here that from the simple estimate of the maximum disc size and peak X-ray luminosity, the outer disc temperature has to be above 11 000 K in the soft and intermediate states, while from the light-curve behaviour we get $T_{\rm eff} \gtrsim 18\,000$ K. Thus, we conservatively assume that $T_{\rm eff} \gtrsim 15\,000$ K during the peak of the 2000 outburst.

2.3 Extinction towards XTE J1550–564 and spectral index–colour relation

Optical extinction towards XTE J1550–564 can be estimated from the hydrogen column density. The FTOOLS routine NH (Dickey & Lockman 1990) gives $N_{\rm H} = 0.9 \times 10^{22}$ cm^{-2}. Tomsick, Corbel & Kaaret (2001) has obtained $N_{\rm H} = (0.85^{+0.22}_{-0.24}) \times 10^{22}$ cm^{-2} using *Chandra* observations in the end of the 2000 outburst. Similar result, $N_{\rm H} = (0.88^{+0.12}_{-0.09}) \times 10^{22}$ cm^{-2}, was obtained by Corbel, Tomsick & Kaaret (2006) again from the *Chandra* observations in a quiescent state. The most accurate measurement of $N_{\rm H} = (0.80 \pm 0.04) \times 10^{22}$ cm^{-2}, which we use for X-ray data analysis, is from the *Chandra* observations during the peak of the 2000 outburst (Miller et al. 2003). Thus, all measurements are consistent with $N_{\rm H}$ lying in the interval $(0.75$–$1) \times 10^{22}$ cm^{-2}. However, these results are inconsistent with the earlier estimate of the extinction $A_V = 2.2 \pm 0.3$ based on interstellar optical absorption lines (Sánchez-Fernández et al. 1999). The later measurements and modelling of Orosz et al. (2011) imply $A_V \approx 4.75$. The Predehl & Schmitt (1995) relation, $A_V = 5.59\,N_{\rm H}/10^{22}$, gives $A_V = 4.2$–5.6.

Another way of estimating A_V is to use constraints on the disc temperature from Section 2.2. We have converted the OIR magnitudes to fluxes and fitted the three-point spectra obtained in the soft and intermediate states with the blackbody disc of the constant radius $R_{\rm irr}$ and varying temperature:

$$F_\nu(T_{\rm eff}) = \cos i \; B_\nu(T_{\rm eff}) \, \pi R_{\rm irr}^2/D^2. \qquad (6)$$
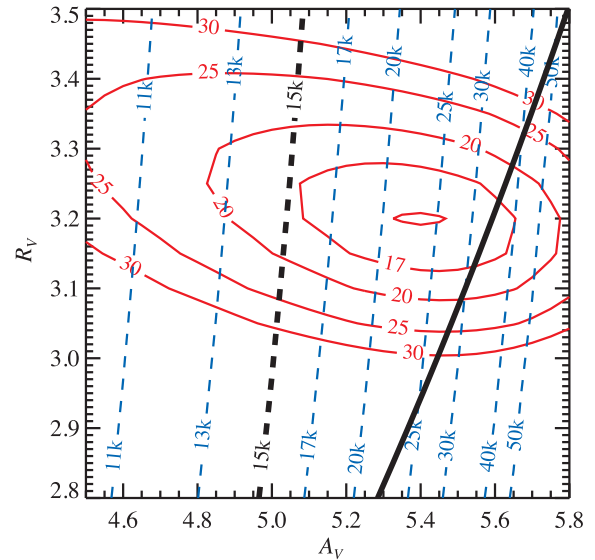
Figure 3. Contours of χ^2 (red solid curves) for the blackbody fit to the OIR data in the soft and intermediate state (MJD 51663–51676) at the plane A_V–R_V. The dashed contour lines show the average temperature in these states varying from about 10 000 K for $A_V = 4.5$ to 30 000 K for $A_V = 5.5$. The thick dashed black line marks the position of the average $T_{\rm eff} = 15\,000$ K, thus the region to the left of this line is forbidden. The region to the right of the thick solid black line corresponds to $\alpha_{VI} > 2$, i.e. harder than the Rayleigh–Jean and therefore is forbidden.

The extinction A_V was allowed to vary. We also checked how the shape of the extinction curve affects the results by varying R_V. We used the extinction law of Cardelli, Clayton & Mathis (1989) corrected by O'Donnell (1994). All together we fitted 13 one-day-averaged spectra (39 points) using 14 fitting parameters ($R_{\rm irr}$ and 13 temperatures) with 25 d.o.f. The contours of χ^2 on the plane R_V–A_V are shown in Fig. 3. We see that the best fit with $\chi^2 = 14.9$ is achieved for $R_V = 3.2$ and $A_V = 5.4$. The effective disc radius is $R_{\rm irr} = 2.85 \times 10^{11}$ cm, which is 40 per cent smaller than the maximal possible disc size limited by tidal forces. We should remember, however, that the actual emission area is likely a ring, not a circular disc, therefore the actual disc size is larger. We also plot at the same plane the average temperature from the best-fitting models. The lower limit on the typical temperature $T_{\rm eff} > 15\,000$ K obtained in Section 2.2 can be now transformed to a lower limit of $A_V > 5.0$. These results are almost independent of R_V.

Two more constraints can be obtained from the extreme colours shown by XTE J1550–564. For that it is useful to get the relations between colours and the corresponding intrinsic (without absorption) spectral indices α of the power-law spectrum $F_\nu \propto \nu^\alpha$. The apparent magnitude in any filter is defined as

$$m_\nu = -2.5 \log F_\nu/F_{\nu,0} + A_\nu, \qquad (7)$$

where A_ν is the extinction, F_ν is the intrinsic flux without absorption and $F_{\nu,0}$ is the zero-point. The slope between bands i and j can be computed as

$$\alpha_{ij} \equiv \frac{\log\left(\frac{F_i}{F_j}\right)}{\log\left(\frac{\nu_{\rm eff,i}}{\nu_{\rm eff,j}}\right)} = \frac{m_i - m_j - A_i + A_j - 2.5 \log\left(\frac{F_{i,0}}{F_{j,0}}\right)}{2.5 \log\left(\frac{\lambda_{\rm eff,i}}{\lambda_{\rm eff,j}}\right)}, \qquad (8)$$

where λ_{eff} are the effective wavelengths of the corresponding filters. The slopes between the considered bands V, I and H are then[1]

$$\alpha_{VH} = 1.16 + 0.69\, A_V - 0.84\, (V - H), \tag{9}$$

$$\alpha_{IH} = 1.21 + 0.55\, A_V - 1.29\, (I - H), \tag{10}$$

$$\alpha_{VI} = 1.07 + 0.94\, A_V - 2.42\, (V - I), \tag{11}$$

where we used the ratios $A_I/A_V = 0.61$ and $A_H/A_V = 0.185$ obtained for $R_V = 3.2$.

The bluest spectra observed from XTE J1550–564 during a brighter outburst in 1998 (Jain et al. 1999), which had $V - I = 1.8$ (for $V = 16.8$ and $I = 15.0$), have to be softer than the Rayleigh–Jean tail of the blackbody, i.e. $\alpha_{VI} < 2$. Using equation (11), we now immediately get a firm upper limit on $A_V \lesssim 5.6 + 0.75\,(R_V - 3.2)$ shown by a thick black solid line in Fig. 3.

On the other hand, the reddest spectra in the beginning and the end of the 2000 outburst still consistent with the blackbody have $V - H \approx 5.3$. According to the disc instability models (Dubus, Hameury & Lasota 2001; Lasota 2001; Frank et al. 2002), for the outburst to start, the outer disc temperature has to be above the hydrogen ionization temperature of about 6000 K. The blackbody of this temperature has $\alpha_{VH} \approx 0.1$. Thus, we get the lower limit from equation (9): $A_V \gtrsim 4.9$, which is nearly identical to the constraint we get from the soft-state spectra in Section 2.2.
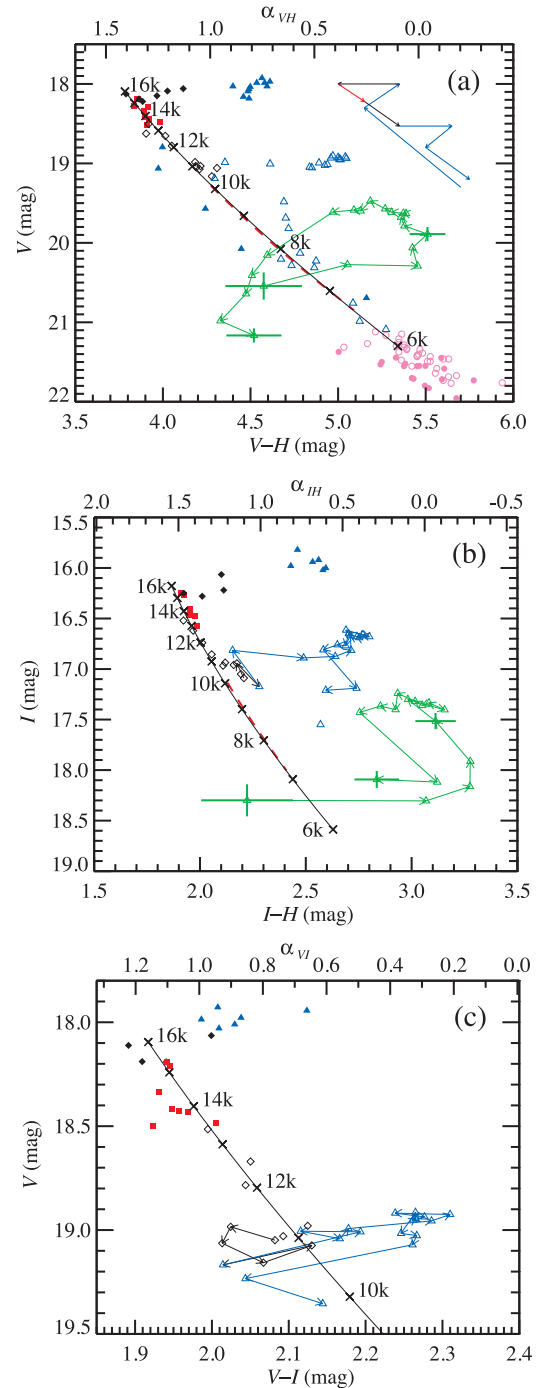
We conclude that a realistic range of the extinction is $A_V = 5.0$–5.6. In the further discussion, we adopt $A_V = 5.0$ (and $R_V = 3.2$), with extinction in other filters is then $A_I = 3.05$ and $A_H = 0.92$. Note that if we assume larger A_V, the typical spectral indices would then be larger than given by equations (9)–(11). This does not change qualitatively the behaviour of the source and does not affect any of the conclusions.

3 SPECTRAL PROPERTIES

3.1 *V* versus *V − H* diagram

Fig. 4(a) represents the V versus $V - H$ colour–magnitude diagram (CMD). The symbols correspond to the outburst stages identified from the X-ray hardness ratio (Fig. 1). The path the source makes on the diagram is illustrated in the upper-right corner with arrows. The black line corresponds to theoretical colour–magnitude relation for a blackbody of different temperatures with the disc radius determined from the best fit to the soft- and intermediate-state spectra (assuming $A_V = 5$). The upper x-axis at the CMD shows the slope α of the intrinsic spectrum between the corresponding bands converted from the colour using equation (9).

At the beginning of the outburst their evolution can be well described by a blackbody of increasing temperature, until the colour $V - H \sim 4.0$ is achieved. After that, the source becomes significantly redder than a blackbody of the corresponding V magnitude. This behaviour can be interpreted as an appearance of an additional,

[1]These transformation laws correct the erroneous expressions presented in Russell et al. (2011), which have wrong scalings and give index α of about 1.0 too small. They have used the wavelength and the zero-point of the J filter instead of those for the H filter in the equation similar to our equation (9), while in the equation corresponding to our equation (10), they have taken the values for the Johnson I filter instead of the Kron–Cousins I filter (Dipankar Maitra and David Russell, private communication).

Figure 4. The observed (a) V versus $V - H$, (b) I versus $I - H$ and (c) V versus $V - I$ CMDs. The coloured track in the upper-right corner of panel (a) illustrates the path XTE J1550–564 follows at the diagram. The black solid lines represent the theoretical curves for the blackbody disc of radius $R_{irr} = 2.85 \times 10^{11}$ cm inclined at $i = 75°$ at distance of 4.38 kpc (Orosz et al. 2011) of different temperatures (in units of thousands of Kelvin, marked next to the line). The model magnitudes were reddened following the extinction law of Cardelli et al. (1989) and O'Donnell (1994) with $A_V = 5$ and $R_V = 3.2$. The upper x-axes show the intrinsic spectral indices in the corresponding wavelength bands given by equations (9)–(11). The red dashed line represents the disc component extrapolated to the time of the flare in the hard state (see Fig. 2). The blue and black arrows connect points in the end of intermediate and beginning of the hard states. The green track shows the path made by the flare component during the hard state starting from MJD 51688 (see Section 3.4).

non-thermal component. At the X-ray hard-to-soft (HS) transition, the source returns to the blackbody track at almost constant *V* magnitude (horizontal track in the CMD), indicating the quenching of the additional component around MJD 51659. In the soft and in the beginning of the following intermediate state, the OIR colours are well described by a blackbody of decreasing temperature. During the reverse transition, we observe re-appearance of the red component around MJD 51683, again as a horizontal track in the CMD. Then the source slowly decays towards the quiescence along the blackbody track of the same normalization as during the soft state, which is, however, slightly larger than that at the rising phase of the outburst. The peculiar fast changes in the *H* band at almost constant *V* band put constraints on the possible origin of non-thermal emission.

We also have checked, whether additional contribution from the secondary star affects the overall shape of the magnitude–colour relation. We used the atmosphere templates of Castelli & Kurucz (2004) for a K3 star with $\log g = 3.5$, $T_{\rm eff} = 4500$ K and radius of $1.75\,R_{\odot}$ (Orosz et al. 2011). The secondary has a minor effect on the CMD, except for quiescence, where the model becomes slightly redder than the data. If, however, we assume a larger extinction, e.g. $A_V = 5.2$, the blackbody temperature corresponding to the soft state increases to 20 000–25 000 K and the total theoretical CMD, then well describes the data even in the quiescent state. Because we are not interested in this state (and for the sake of simplicity of the model), we further do not account for the secondary contribution.

3.2 *I* versus *I − H* diagram

We also plot the *I* versus *I − H* CMD in Fig. 4(b). The behaviour of the source in this diagram is very similar to that in the *V* versus *V − H* CMD. The blackbody track (black solid line) for the same parameters as in Fig. 4(a) provides a good fit to the data from MJD 51660 at the end of the hard-to-soft (HS) transition, in the soft state and in the beginning of the soft-to-hard (SH) transition until about MJD 51683. In the middle of the SH transition, the source becomes redder indicating the presence of the additional component. The X-ray hardness during the moments of appearance/disappearance of this component was nearly the same (see Fig. 1 c), corresponding to the X-ray spectrum with photon index $\Gamma \approx 1.9$ and reflection amplitude $\Omega/(2\pi) \approx 1$.

An interesting additional detail is a hook-like evolution (marked by blue arrows) at the end of the hard state, before the flare in the *H* filter. This feature arises because several data points at the beginning of the hard state are redder at lower *I* flux compared to the data points a few days later, which makes the spectrum bluer (larger α_{IH}) at a higher *I* flux. This behaviour cannot be an artefact of interpolation between non-simultaneous points in the *H* filter and can be interpreted as the flare starting first in the *I* band, then proceeding to the *H* band. This is consistent with the shape of the flare spectra (see Section 3.4 and Fig. 5).

The spectral index α_{IH} (upper *x*-axis) at the peak of the flare (when the spectrum is softest in the hard state) is identical to α_{VH}, implying a single power-law component going through all three filters. We note that taking larger values of extinction results in a larger α (harder spectra), but the effect is larger for α_{VH} than for α_{IH}, thus the spectrum would no longer be described by a single power law.
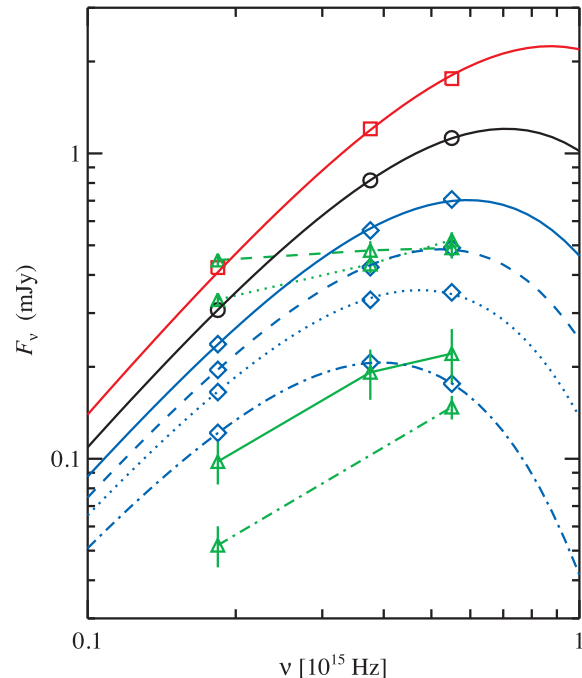
Figure 5. Examples of spectra (corrected for extinction) and the best-fitting blackbody model of constant emission area. Data taken in the soft state on MJD 51665 and in the intermediate state on MJD 51676 are shown by red squares and black circles, respectively. In the hard state, the disc fluxes on MJD 51688, 51697, 51706 and 51726 obtained by interpolation are shown by blue diamonds and the flare component by green triangles. The best-fitting blackbody models are shown by solid, dashed, dotted, dot–dashed blue lines, respectively. The errors are not shown for most data points, because they are smaller than the size of the symbols.

3.3 *V* versus *V − I* diagram

The general evolution of the source at the *V* versus *V − I* CMD shown in Fig. 4(c) is very similar to those for other filters as described above. However, at this diagram the appearance of the additional non-thermal component is easier to see. Around MJD 51683, in the middle of the intermediate state, the spectrum becomes bluer, which is reflected in motion of the source at $V = 19$ to the left from the blackbody model line by $\Delta(V − I) \approx 0.1$ (shown by black arrows). This implies that the additional component has a spectrum harder than the blackbody spectrum at this moment of $\alpha_{VI} \approx 0.7$. The spectrum becomes redder that the corresponding blackbody at MJD 51688. Only at this moment, the flare starts to become easily visible in the light curves.

3.4 Flares and the non-thermal component

The underlying behaviour of light curves in *V*, *I* and *H* filters is naturally explained with the evolving temperature of the accretion disc, which responds to changes in the X-ray luminosity (i.e. due to changes of the reprocessing flux). The CMDs as well as the spectra at the soft and the following intermediate states suggest that the OIR emission comes from the irradiated accretion disc that is modelled here as a blackbody (see Fig. 5 and Sections 3.1 and 3.2). The flares that occur in the intermediate/hard states can be interpreted as the appearance of an additional, non-thermal component. The first flare starts at the rising phase of the outburst and it is therefore impossible to separate it from the underlying disc emission. On the other hand, the second flare occurs at the exponentially decaying stage and it is

possible to subtract the disc emission in order to isolate the flaring component.

To obtain the disc emission at the time of the second flare, we use the same model as in Section 2.2, i.e. we fit the light curves in every filter with the constant plus exponential that represents the irradiated disc. The fit is applied to the times MJD 51663–51683 for all filters and MJD 51750–51755 for *V* and *H* filters. The first interval correspond to the soft and intermediate states where there no signatures of the additional component, while the second interval correspond to the quiescent state. Unfortunately, no *I*-filter data exist after MJD 51717 and similarly to Section 2.2, we fix the constant corresponding to $I = 19$. The best-fitting models are shown in Fig. 2 by dashed red curves. After the fitting, we check that the magnitudes and colours of the extrapolated disc component are consistent with the blackbody of the same size as before the flare (compare red dashed lines in Fig. 4 to the black solid lines representing the blackbody model). We see that the typical accuracy of the magnitudes of the interpolated blackbody component is better than 0.03.

By subtracting the blackbody flux at every moment, we extract the flaring non-thermal component. The evolution of colours and spectral indices of the flare is shown in Fig. 4 by green triangles connected by arrows. The typical errors are shown by crosses for a few points. From Fig. 4(a), we see that the flare starts with the hard index $\alpha_{VH} = 0.75 \pm 0.20$, then softens down to $\alpha_{VH} \approx 0$ and then hardens again to $\alpha_{VH} = 0.7 - 0.8$. The time evolution of α_{VH} of the total spectrum and of the flaring component is shown in the middle and lower panels of Fig. 2.

The flare path in *I* and *H* filters is seen in Fig. 4(b). The evolution is similar to the $V - H$ colours, but the spectrum is even harder at the start of the flare with $\alpha_{IH} = 1.1 \pm 0.3$, implying that the spectrum hardens towards longer wavelengths (see green solid line in Fig. 5). At the peak of the flare $\alpha_{IH} \approx +0.2$ nearly identical to α_{VH} implying that the spectrum in three filters is close to a power law of the same index. At the end of the flare, the spectrum in *I* and *H* band is less reliable, because of the growing error in the disc flux in *I* filter.

The flare becomes visible in the light curves only in the beginning of the hard state at MJD 51688, but substantial deviations from the blackbody spectrum occur already at MJD 51683 as can be seen from the $V - I$ colour evolution shown in Fig. 4(c). In the end of intermediate state, during MJD 51683–51687 the total spectrum is bluer than the blackbody with $\alpha_{VI} \approx 0.7$ and reaches $\alpha_{VI} \approx 1$. This implies that the slope of the flare spectrum between *I* and *V* filters is substantially larger than unity, because the flare contribution to the total flux at this moment is still rather low.

Fig. 5 demonstrates the evolution of the disc and the flare spectra during the outburst. We see that the flare spectrum is a broken power law just at the start of the flare, but is consistent later with a simple power law. Assuming a larger extinction, e.g. $A_V = 5.2$, results in α larger by about 0.2, but the qualitative behaviour remains the same. We note here that our conclusions on the evolution of the flare spectrum are based on the assumption that the blackbody normalization did not change during the decaying phase of the outburst. This is supported by the absence of significant variations in the normalization from the soft state to the end of the hard state as well as the quiescence.

3.5 OIR–X-ray relation

Once we have separated the non-thermal component in the OIR band, it is worth looking at a larger picture by understanding the relation between the OIR flare spectrum and the X-rays. Fig. 6
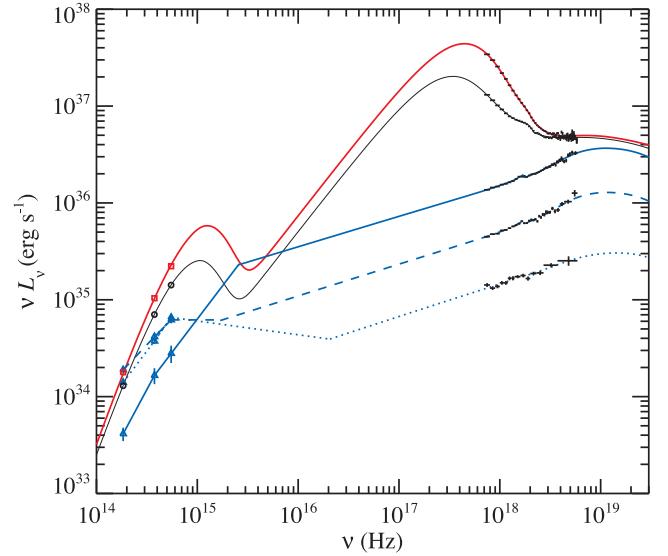
Figure 6. Broad-band OIR to the X-ray spectral energy distribution of XTE J1550–564. The black crosses are the *RXTE*/PCA data. Spectra are plotted for the same dates as in Fig. 5, excluding the last one, which has very unreliable X-ray spectrum because of the strong background due to the Galactic ridge emission. The soft state data at MJD 51665 and the model are shown by red squares and the curve, the intermediate state at MJD 51676 (black symbols), and the hard-state data at MJD 51688, 51697 and 51706 by blue triangles and by solid, dashed and dotted curves, respectively. The blackbody component from the irradiated disc is shown in the OIR for the soft and intermediate states, while for the hard state only the flare component (same as in Fig. 5) is shown. The hard-state OIR model spectra are somewhat arbitrarily connected to the power law extrapolated from the X-ray data.

shows the broad-band OIR/X-ray spectra of XTE J1550–564 taken at different states. Similar X-ray data from the 2000 outburst of XTE J1550–564 were presented before by Yuan et al. (2007) and Xue, Wu & Cui (2008).

The soft-state X-ray spectrum (taken on MJD 51665) is dominated by a strong thermal component from the optically thick accretion disc. There is a high-energy tail above 20 keV. These non-thermal tails are well explained by non-thermal Comptonization in the hot corona above the disc (Poutanen & Coppi 1998; Gierliński et al. 1999; Zdziarski & Gierliński 2004). The thermally looking component itself cannot be explained by a simple standard disc model, but requires a contribution from thermal Comptonization. The whole X-ray spectrum thus can be fitted with a hybrid Comptonization model such as EQPAIR (Coppi 1999) or COMPPS (Poutanen & Svensson 1996) models in XSPEC. Here, we used the latter. We do not discuss here the best-fitting parameters of the model, just because the aim of the fitting is only to show the shape of the spectrum, which is rather independent of the model choice. The extrapolation of the standard cold accretion disc DISKBB spectrum to lower energies reveals that it cannot contribute more than a few per cent to the observed OIR flux, which is dominated by the reprocessed radiation from the outer disc with the total (unabsorbed) luminosity of $L_{\rm repr} \approx 7.3 \times 10^{35}$ erg s^{-1}. This has to be compared to the total (unabsorbed) X-ray luminosity in the 0.01–1000 keV band of $L_{\rm X} \approx 1.2 \times 10^{38}$ erg s^{-1}. Assuming the same angular dependence of radiation for both components, the ratio of luminosities gives the total reprocessing efficiency of $\epsilon_{\rm repr} \approx 6 \times 10^{-3}$. The intermediate-state spectrum (on MJD 51676) is nearly identical to the soft-state spectrum, with a slightly lower temperatures and the X-ray and outer disc luminosities of $L_{\rm X} \approx 7.1 \times 10^{37}$ erg s^{-1} and $L_{\rm repr} \approx 3.2 \times 10^{35}$

erg s^{-1}, respectively, giving nearly the same reprocessing efficiency of $\epsilon_{repr} \approx 4.5 \times 10^{-3}$.

In the hard state, we used the cutoff power-law model with Compton reflection (PEXRAV model in XSPEC; Magdziarz & Zdziarski 1995) for modelling and estimating the luminosities, because there are no any signatures of the thermal emission from the standard accretion disc in the X-ray band. We assumed a cutoff at 200 keV which is typical for a BH X-ray binary. During the three considered days (MJD 51688, 51697 and 51706), the spectral shape varied very little, with the power-law photon index being nearly identical at $\Gamma \approx 1.65$ (i.e. $\alpha \approx -0.65$) and the reflection amplitude $\Omega/(2\pi)$ decreasing from about unity to 0.3. The X-ray luminosity took the values of $L_X \approx (16, 5.6, 1.5) \times 10^{36}$ erg s^{-1}. The X-ray spectrum taken on MJD 51697 extrapolated to the OIR band (see blue lines in Fig. 6, where we plotted only the flare spectrum in the OIR) matches rather well with the OIR power law. At the beginning of the hard state, at MJD 51688 (solid blue line), the extrapolation of the X-ray power law is an order-of-magnitude above the OIR flux. On the other hand, later in the hard state, on MJD 51706, the X-rays underpredict the OIR emission.

In addition to the flare component, the emission from the irradiated disc (not shown in Fig. 6) was also steadily declining with $L_{repr} \approx (16, 9.5, 6.3) \times 10^{34}$ erg s^{-1} at the same three dates. This gives the reprocessing efficiency of $\epsilon_{repr} \approx (1, 1.7, 4.2) \times 10^{-2}$. Thus, we see a clear trend of increasing ϵ_{repr} with decreasing X-ray luminosity. This trend has also been reported for other BH transients (e.g. Gierliński et al. 2009). There could be at least two reasons for such a change. First, the geometry of the accretion disc and therefore the emission pattern changes during the SH transition. In the soft state, the emission from optically thick standard disc is beamed perpendicular to its plane, hence the outer disc sees less radiation than the observer at 75° inclination. In the hard state, however, the emission from optically thin hot disc is much more isotropic (see e.g. Veledina, Poutanen & Ingram 2013b). Secondly, the reprocessing efficiency is higher for harder spectra, because the soft X-rays are absorbed in the very surface layers producing mostly UV lines and recombination continua (Suleimanov et al. 1999; see also discussion in Gierliński et al. 2009). We can account for the second effect by dividing L_{repr} by the luminosity above 2 keV, getting the reprocessing efficiency of $\epsilon_{repr} \approx 1.2 \times 10^{-2}$ and 0.8×10^{-2} in the soft and intermediate states, respectively, and $\epsilon_{repr} \approx (1.2, 2.1, 5.2) \times 10^{-2}$ in the hard state. This reprocessing efficiency is still rather modest because for the disc half-opening angle of 12° (de Jong et al. 1996), we expect $\epsilon_{repr} \lesssim 0.15$ assuming albedo of 0.3. The observed reprocessing efficiency can actually be even lower, because at low fluxes a significant fraction of the OIR radiation can be produced by the (ignored here) secondary star and/or the bulge located at the impact point of the accretion stream.

4 ORIGIN OF NON-THERMAL COMPONENT

4.1 Jet?

The non-thermal OIR component seen in XTE J1550–564 was attributed to the jet synchrotron emission in a number of works (Corbel et al. 2001; Russell et al. 2010, 2011). The aforementioned works used the optical data, originally published in Jain et al. (2001b), the same as used in this work. Corbel et al. (2001) obtained optical $V - I$ spectral index $\alpha = -2.6$ (assuming $A_V = 2.2$) on 2000 June 1 (MJD 51697), in contrast to the obtained by us the flare spectral index

$\alpha \approx 0$ (for $A_V = 5.0$). The source of discrepancy is the extinction value, poorly known at that time.

The studies by Russell et al. (2010, 2011) present the separation of the non-thermal emission using the light-curve fitting method. They claimed that the spectral indices of the non-thermal component are in the range $-1.5 \lesssim \alpha \lesssim -0.5$, again suggesting the non-thermal optically thin jet emission. However, these works suffer from the major errors in formulae for transformation of the colours to indices (see Section 2.3). Furthermore, their fits to the disc light curve in V and I filters are significantly above the data points just before the flare (see fig. 2 in Russell et al. 2010) leading to overestimation of the disc contribution and to oversubtraction of the flux in those filters resulting in a much too soft flare spectrum. These flawed fits have greatly affected the first few points of the flare, where the non-thermal V flux was small, hence only spectral hardening during the flare was detected, while we obtain that the flare starts with hard spectrum with $\alpha \approx +0.75$, which softens to $\alpha \approx 0$ and then hardens again (see Fig. 4). Such behaviour is clearly inconsistent with the optically thin jet spectrum. The jet radio emission was indeed optically thin in the soft state, with $\alpha_{radio} = -0.46 \pm 0.03$ (Fig. 7), but it does not contribute at all to the OIR spectrum, which was consistent with the blackbody.

On the other hand, the radio emission in the hard state close to the peak of the second flare, on MJD 51697.14 was optically thick with $\alpha_{radio} = 0.36 \pm 0.09$ (Corbel et al. 2001). However, the OIR flare spectrum has a different slope and does not lie on the continuation of the radio spectrum (see green points in Fig. 7). Connecting those requires a break in the spectrum in the far-IR, which is inconsistent with the simplest jet models where main parameters follow the power-law radial dependences with constant indices (Blandford & König 1979; König 1981). The strongest arguments against the jet contribution to the OIR, however, come from the rather hard OIR spectra of the flare. First, the hook-like behaviour on the $I - H$ CMD at the beginning of the flare (Fig. 4 b), a broken power-law flare spectrum which hardens towards red on MJD 51688 (greed solid line in Fig. 5) as well as the hard flare spectrum with $\alpha > 1$ in the end of the intermediate state (see Section 3.3 and Fig. 4 c) are not consistent with the jet spectrum extending from radio to the OIR band. Secondly, later in the hard state, the flare spectrum has $\alpha \sim 1$. If it were optically thick jet emission, the radio flux would be about five orders of magnitude below what was observed just a few days before. We find this highly improbable. Furthermore, it is difficult to understand how a substantial decrease in the accretion rate could lead to formation of the outflow which is optically thick up to the OIR band. The weakness of the jet in the OIR band also implies that the jet cannot possibly contribute to the X-rays.

OIR flares were observed in a number of BH X-ray binaries. It was noticed that the beginning of the flare nearly coincides with the radio brightening (Kalemci et al. 2013). We find that the position of XTE J1550–564 at the X-ray hardness–flux diagram at the times of quenching/recovery of the OIR non-thermal component (see Fig. 1 c) closely resembles the 'jet line' (Belloni, Motta & Muñoz-Darias 2011). This coincidence can be interpreted in two alternative ways: (i) both OIR and radio emission originate from one component (jet), or (ii) both are causally connected, but originate in different places. As we showed above, the first interpretation is at odds with the spectral evolution of the OIR flare. In the second interpretation, the OIR flare may originate in the geometrically thick hot flow (see below), while the radio is produced in the jet. The coincidence can be interpreted as a simultaneous appearance of the hot flow and the jet. This is indeed expected as in modern MHD simulations the jet seems to form only if there is collimation by a geometrically thick
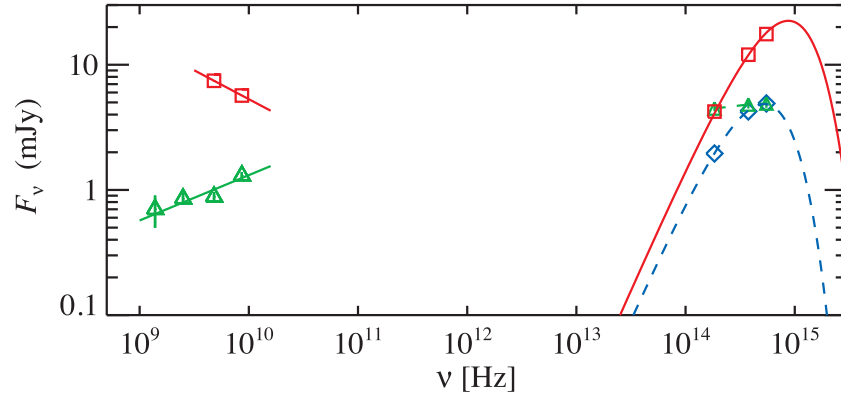
Figure 7. Broad-band radio to optical spectral energy distribution of XTE J1550–564 at MJD 51665 (red squares) and 51697 (green triangles and blue diamonds). The radio data are taken from Corbel et al. (2001) and the OIR data from Jain et al. (2001b). We plot the blackbody with temperature and normalization as inferred from the light curves and the CMD. The additional emission is due to the non-thermal component (shown with green symbols). In the soft state, the radio jet does not contribute at all to the OIR band, and in the hard state the flare OIR spectrum has a different slope $\alpha \approx 0$ that does not lie on the continuation of the radio power law with $\alpha_{\mathrm{radio}} \approx 0.36$.

accretion flow. In the soft state, when the cold, geometrically thin disc extends all the way to the innermost stable orbit, the jet is weak.

4.2 Hot accretion flow

It was usually assumed that the electrons in the hot flow follow thermal distribution and in that case synchrotron emission in luminous BH X-ray binaries cannot possibly be of importance (Wardziński & Zdziarski 2000), because of strong self-absorption. However, even if the flow contains a small, energetically unimportant tail of non-thermal electrons, situation changes dramatically, as the synchrotron luminosity increases by orders of magnitude (Wardziński & Zdziarski 2001; Veledina et al. 2013a). This results in two effects: first, the seed photons for Comptonization in the hot flow now can be dominated by the non-thermal synchrotron instead of the cold truncated accretion disc (Malzac & Belmont 2009; Poutanen & Vurm 2009) and, secondly, the synchrotron radiation can dominate the OIR emission from the BH (Veledina et al. 2013a; Poutanen & Veledina 2014). The range of wavelengths where the hot flow emits is determined by its size: the larger is the truncation radius of the cold accretion disc, the lower is the frequency where synchrotron radiation is still not absorbed. The self-absorption (turn-over) frequency is (Veledina et al. 2013a)

$$\nu_t \approx 3 \times 10^{15} (B/10^6\,\mathrm{G})^{(p+2)/(p+4)} \, [\tau(p-1)]^{2/(p+4)} \ \mathrm{Hz}, \qquad (12)$$

where B is the magnetic field strength, τ is the Thomson optical depth of non-thermal electrons and p is the slope the electron distribution.

For the radial dependences $B \propto R^{-\beta}$ and $\tau \propto R^{-\theta}$ the self-absorption frequency scales as $\nu_t \propto R^{-[\beta(p+2)+2\theta]/(p+4)}$ and the total OIR spectrum from a hot flow is composed of contributions of synchrotron peaks (in partially opaque regime) coming from different radii. The hot flow spectrum constitutes a power law with the spectral index (Veledina et al. 2013a)

$$\alpha_{\mathrm{OIR}} = \frac{5\theta + \beta(2p+3) - 2p - 8}{\beta(p+2) + 2\theta}. \qquad (13)$$

At frequencies above ν_t for the smallest, most compact zone of the accretion disc, the synchrotron spectrum is optically thin with $\alpha = -(p-1)/2$. If the optical depth of thermal electrons is high enough, thermal Comptonization can dominate completely over the optically thin synchrotron, the latter therefore might be invisi-

ble in the total spectrum. At frequencies below the self-absorption frequency for the largest, most transparent zone, the spectrum is optically thick with $\alpha = 5/2$.

Below we follow the hybrid hot flow scenario as described in details in Veledina et al. (2013a). We discuss now how it can explain the broad-band spectrum and the features seen in the CMD. We also discuss what are the implications for the physical parameters in the vicinity of the BH.

4.2.1 Broad-band spectrum

The broad-band OIR-to-X-ray spectra in the soft and intermediate states are fully consistent with the standard accretion disc with the addition of the emission from non-thermal/hybrid electrons in the hard X-rays and the irradiated disc in the OIR band (see Fig. 6). The X-ray non-thermal emission can presumably be associated with the corona above the accretion disc, as in these states the hot inner flow either is non-existent or very small. Because of high luminosity of the standard disc, electron cooling is dominated by Compton scattering, hence the synchrotron component from the corona is negligible. Indeed, there are no any signatures of this emission in the OIR band.

In the hard state, the whole OIR to X-ray spectrum can be explained by a synchrotron self-Compton model where the synchrotron emission from non-thermal electrons is Comptonized by the thermal population of electrons (Poutanen & Vurm 2009; Veledina et al. 2013a). At the beginning of the hard state (MJD 51688), the accretion rate $\dot{M}$ is high, the synchrotron self-absorption frequency of the innermost zone is at $\approx 3 \times 10^{15}$ Hz (corresponding to $B \sim 10^6$ G and $\tau \sim 1$, see equation 12), while $\nu_t \sim 3 \times 10^{14}$ Hz for the outermost zone of the hot flow resulting in a break to harder spectrum below that frequency. This explains a fact that the extrapolation of the X-ray power law overpredicts the OIR flux (solid blue lines in Fig. 6). Later in the hard state, during the peak of the OIR flare (on MJD 51697), $\dot{M}$ and therefore B and τ have dropped, the hot flow has grown in size and ν_t for both inner- and outermost zones have decreased. This results in a flat power-law spectrum in the OIR band (see dashed blue lines in Fig. 6 and the SH transition in Fig. 8 for a schematic presentation of the spectral evolution). Because at lower $\dot{M}$ the total optical depth has likely decreased, the synchrotron peak became more pronounced. Later in the hard
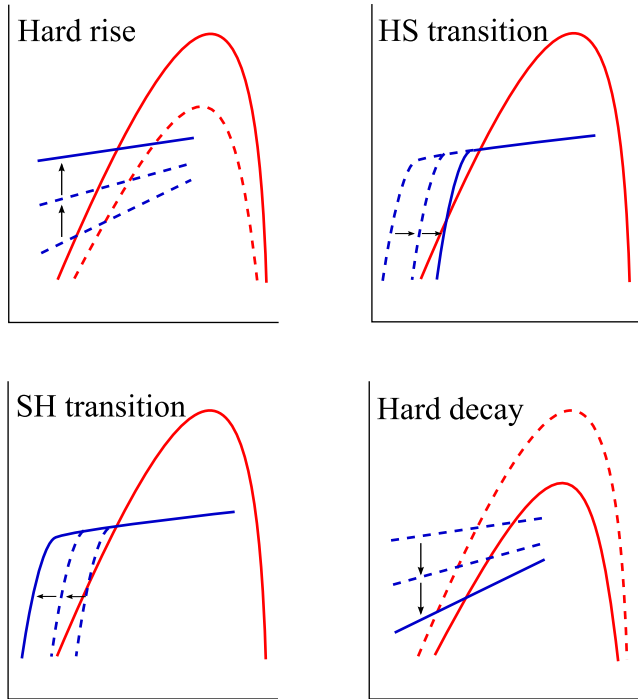
Figure 8. The schematic evolution of the OIR spectra of the irradiated disc and the flare components from the hot flow during the outburst. At the rising phase of the outburst, in the hard state, the disc temperature is steadily growing together with the luminosity of the non-thermal component. At the HS transition, the X-ray luminosity is nearly constant resulting in a nearly constant disc emission; the hot flow size shrinks affecting the synchrotron self-absorption frequency, which is increasing. At the soft state (not shown here), the non-thermal synchrotron component may not exist at all, because the hot flow has disappeared. At the SH transition, the hot flow appears and its size steadily grows resulting in a rapid evolution of the self-absorption frequency. In the following hard state, the X-ray as well as the disc luminosity drop; the non-thermal component decays even faster and becomes harder.

state (on MJD 51706; dotted blue lines in Fig. 6), when the optical depth in the hot flow drops further, the OIR/X-ray spectrum cannot be represented by a broken power law any longer. Instead, it seems that there are two bumps in the OIR and the X-rays (similar to the spectra of blazars). Such double-peaked spectra are generally expected in the hot flow scenario at luminosities below a few per cent of the Eddington, at low optical depths (see fig. 6 in Narayan, Mahadevan & Quataert 1998 and fig. 5 in Veledina, Vurm & Poutanen 2011a).

4.2.2 Horizontal tracks in CMD

The OIR spectrum of the hot flow constitutes a power law, which extends down to the self-absorption frequency ν_t of the outermost parts. During the rising phase of the outburst, the cold accretion disc shrinks, gradually replacing the hot flow at smaller and smaller radii. Thus, ν_t shifts to higher frequencies (see Fig. 8). Once the ν_t crosses the H filter, the emission at these wavelengths becomes self-absorbed and further, even rather small increase of the transition frequency results in rapid decrease of the H flux. At the same time, the V filter experiences minor changes, until the ν_t reaches it. At the decay phase of the outburst, the cold disc recedes, thus the transition frequency moves towards longer wavelengths, and the rapid flux increase in H filter occurs. This behaviour naturally explains the horizontal tracks we see in the CMDs (Fig. 4).

The V–I CMD (Fig. 4 c) also shows a nearly horizontal movement but to the left of the blackbody track in the end of the SH transition corresponding to the hardening of the spectrum. This is a natural consequence of the appearance of a hard hot flow component which compensates the decreasing disc flux in the V filter but does not contribute much to the I filter.

It is interesting to note that the horizontal tracks appear at different luminosities. These levels correspond to a factor of 1.35 difference in the outer accretion disc temperature, while the X-ray HS and SH transitions occur at luminosities that differ by a factor of 3. This is consistent with a simple relation $T_{\rm eff} \propto L_{\rm X}^{1/4}$. Thus, the horizontal tracks in the OIR CMDs and the X-ray hysteresis loop are both manifestation of the same phenomenon. We finally note that the hot flow emission in the OIR band disappears/appears in the intermediate states at the rising and decaying stages of the outburst around MJD 51659 and 51683, respectively (see Figs 4 b,c), at a similar X-ray hardness (see Fig. 1 c). This strongly argues in favour of a similar truncation radius of the cold disc at these moments in spite of a factor of three difference in X-ray luminosity.

4.2.3 $I - H$ hook

At the HS transition, when the cold disc truncation radius decreases, hot flow model predicts a quenching of the emission at longer wavelengths before that at shorter wavelengths. For instance, quenching the emission in the H filter results in a rapid colour change at an almost constant I magnitude, as indeed seen in the I versus $I - H$ CMD (Fig. 4 b). Then, quenching of the emission in I filter is expected, however, it is more difficult to see in this diagram, because both the magnitude and the colour change, at the same time the thermal emission is increased, partially compensating for the drop in I filter. The behaviour is tentatively seen in Fig. 4(b), where the return to the blackbody track goes along the horizontal line (at constant I), then the I flux also decreases. However, due to large error bars and small number of data points, the evolution is also consistent with a decrease of the emission in both filters, I and H.

The situation is different at the reverse, SH transition. With receding cold disc, the hot flow emission is recovered at shorter wavelengths before longer wavelengths. We thus expect the evolution to proceed as follows: first, the spectrum follows a cooling blackbody, then the I flux increases, thus both colour and magnitude change in the opposite direction (towards upper left in Fig. 4 b), then the H flux increases and the horizontal track appears. Such a behaviour is indeed seen as a hook at the $I - H$ CMD. The rise of the emission in the I filter before the H filter cannot be accounted for by the jet model. It is thus a good proxy for discriminating between the jet and the hot flow scenario.

4.2.4 Hot flow size and radial structure

When the OIR flare becomes visible in the very beginning of the hard state at the decaying stage of the outburst, the non-thermal component has spectral index $\alpha_{IH} \approx 1$, which is smaller than the value 2.5 corresponding to the self-absorbed spectrum. This indicates that ν_t lies between the I and H filters. Approximating the hot flow spectrum at these wavelengths with a broken power law (see Fig. 5), we obtain $\nu_t \approx 3 \times 10^{14}$ Hz, from which we can infer the hot flow size at this moment of time. Using equation 13 of Veledina et al. (2013a), which was derived under an assumption of power-law

radial dependences of the magnetic field strength and the electron density, we get

$$R = 3 \times 10^{22}/\nu_t \approx 10^8 \text{ cm} \approx 35 R_S, \qquad (14)$$

where $R_S = 2GM/c^2 = 2.7 \times 10^6$ cm is the Schwarzschild radius of the $9.1 M_\odot$ BH. This value should be considered as a rough estimate, to be improved by detailed spectral modelling.

We find that the non-thermal spectrum does not stay power law of one particular spectral index, but is hardening towards the end of the flare. According to equation (13), α depends on indices θ, β and p. Let us assume that changes in α are predominantly caused by changes in the radial distribution of the optical depth, while β is fixed at a value of 5/4 for advective flows (Shadmehri & Khajenabi 2005). For softest $\alpha = 0.0$ and hardest $\alpha = 1.0$, we obtain a change of θ from ~ 0.55 to 3.0 if we fix $p = 3$ (the precise value has minor effect on the results). The value of θ for the soft spectrum is similar to that found in ADAF flows (Kato, Fukue & Mineshige 2008), however, the value obtained from the hard spectrum is quite an extreme, as it requires a highly inhomogeneous configuration. We should remember, however, that here θ describes the distribution of non-thermal electrons, not their bulk. Thus, high values of θ might imply that electron acceleration is not efficient at large radii. If instead we choose to fix $\theta = 0.5$, we get $\beta = 1.3$ for the soft spectrum (which is close to the standard value in ADAFs), while for the hard spectrum we get $\beta = 3.1$, again suggesting an extreme stratification of the magnetic field strength. In reality, the structure of both the magnetic field and the optical depth is likely to change when the accretion rate decreases, with the general trend, apparent from the above exercise, such that the flow becomes more stratified with strong gradients.

5 SUMMARY

We have carefully analysed the OIR and X-ray light curves of XTE J1550–564. From the e-folding times in different wavebands, we obtained the outer accretion disc temperature in excess of 15 000 K during the soft/intermediate states. Using this temperature together with the extreme OIR colours observed from XTE J1550–564, we put strong constraints on the extinction towards the source, $5.0 \lesssim A_V \lesssim 5.6$. This allowed us to relate the observed OIR colours to the slopes of the intrinsic spectrum.

During the soft state, the OIR spectrum is well described by the blackbody (associated with the irradiated disc) of exponentially decaying temperature and a constant normalization, while during the X-ray state transitions and the hard states, strong non-thermal flares are observed. By interpolating the decaying flux of thermal emission to the hard state, we have accurately separated the contribution of the flare from the disc. Importantly, the spectrum of the subtracted thermal component was shown to be consistent with the blackbody of the same normalization as before the flare. We further demonstrated how the spectrum of the non-thermal component evolves. On the decaying phase of the outburst, the flare starts with an apparent break in the spectrum that is harder in the near-IR with $\alpha \approx 1$. The spectrum then becomes a power law and softens to $\alpha \approx 0$ at the peak of the flare. It hardens again as the source fades. In the hybrid hot flow scenario, this hardening possibly indicates that the electron acceleration is not efficient at large radii at low accretion rates.

The evolution of the spectral shape is consistent with the hot accretion flow scenario, where the size of the flow varies with the accretion rate. In the hard state, the flow is large and the OIR spectrum constitutes a power law. During the HS transition, the flow collapses and the low-energy spectral cutoff (corresponding to the synchrotron self-absorption frequency) moves from the infrared to the UV. In the soft state, the hot flow may not exist at all and its non-thermal emission is quenched. At the reverse transition, the cold disc retreats and the hot flow grows in size leading to an increase of the contribution of the non-thermal component from the hot flow to the OIR spectrum and strong reddening of the source. This transition occurs at a lower accretion rate which manifests itself as the hysteresis loop in the X-ray hardness–flux diagram and as different levels of the horizontal tracks in the OIR CMDs. We find that quenching and recovery of the hot flow OIR emission occurs at about the same X-ray hardness during the intermediate state. The position of the source at the X-ray hardness–flux diagram when this happens (the hot flow line) seems to coincide with the jet line that marks the presence of the compact radio jet. This implies a close connection between the presence of the hot flow and the compact jet. We roughly estimate the hot flow size, at the moment when OIR flare starts to be visible in the light curves, to be 10^8cm $\approx 35 R_S$.

REFERENCES

Arnaud K. A., 1996, in Jacoby G. H., Barnes J., eds, ASP Conf. Ser. Vol. 101, Astronomical Data Analysis Software and Systems V. Astron. Soc. Pac., San Francisco, p. 17
Basko M. M., Sunyaev R. A., Titarchuk L. G., 1974, A&A, 31, 249
Belloni T. M., Motta S. E., Muñoz-Darias T., 2011, Bull. Astron. Soc. India, 39, 409
Bessell M. S., Castelli F., Plez B., 1998, A&A, 333, 231
Blandford R. D., Königl A., 1979, ApJ, 232, 34
Cardelli J. A., Clayton G. C., Mathis J. S., 1989, ApJ, 345, 245
Castelli F., Kurucz R. L., 2004, preprint (astro-ph/0405087)
Chaty S., Haswell C. A., Malzac J., Hynes R. I., Shrader C. R., Cui W., 2003, MNRAS, 346, 689
Coppi P. S., 1999, in Poutanen J., Svensson R., eds, ASP Conf. Ser. Vol. 161, High Energy Processes in Accreting Black Holes. Astron. Soc. Pac., San Francisco, p. 375
Corbel S. et al., 2001, ApJ, 554, 43
Corbel S., Tomsick J. A., Kaaret P., 2006, ApJ, 636, 971
Cunningham C., 1976, ApJ, 208, 534
de Jong J. A., van Paradijs J., Augusteijn T., 1996, A&A, 314, 484
Dickey J. M., Lockman F. J., 1990, ARA&A, 28, 215
Dubus G., Hameury J.-M., Lasota J.-P., 2001, A&A, 373, 251
Durant M., Gandhi P., Shahbaz T., Fabian A. P., Miller J., Dhillon V. S., Marsh T. R., 2008, ApJ, 682, L45
Eggleton P. P., 1983, ApJ, 268, 368
Endal A. S., Devinney E. J., Sofia S., 1976, Astrophys. Lett., 17, 131
Frank J., King A., Raine D. J., 2002, Accretion Power in Astrophysics. Cambridge Univ. Press, Cambridge

Gallo E., Migliari S., Markoff S., Tomsick J. A., Bailyn C. D., Berta S., Fender R., Miller-Jones J. C. A., 2007, ApJ, 670, 600

Gandhi P. et al., 2010, MNRAS, 407, 2166

Gelino D. M., Gelino C. R., Harrison T. E., 2010, ApJ, 718, 1

Gierliński M., Zdziarski A. A., Poutanen J., Coppi P. S., Ebisawa K., Johnson W. N., 1999, MNRAS, 309, 496

Gierliński M., Done C., Page K., 2009, MNRAS, 392, 1106

Hynes R. I., Mauche C. W., Haswell C. A., Shrader C. R., Cui W., Chaty S., 2000, ApJ, 539, L37

Hynes R. I., Haswell C. A., Chaty S., Shrader C. R., Cui W., 2002, MNRAS, 331, 169

Jahoda K., Markwardt C. B., Radeva Y., Rots A. H., Stark M. J., Swank J. H., Strohmayer T. E., Zhang W., 2006, ApJS, 163, 401

Jain R. K., Bailyn C. D., Orosz J. A., Remillard R. A., McClintock J. E., 1999, ApJ, 517, L131

Jain R. K., Bailyn C. D., Orosz J. A., McClintock J. E., Sobczak G. J., Remillard R. A., 2001a, ApJ, 546, 1086

Jain R. K., Bailyn C. D., Orosz J. A., McClintock J. E., Remillard R. A., 2001b, ApJ, 554, L181

Kalemci E., Dinçer T., Tomsick J. A., Buxton M. M., Bailyn C. D., Chun Y. Y., 2013, ApJ, 779, 95

Kanbach G., Straubmeier C., Spruit H. C., Belloni T., 2001, Nature, 414, 180

Kato S., Fukue J., Mineshige S., 2008, Black-Hole Accretion Disks — Towards a New Paradigm. Kyoto Univ. Press, Kyoto

Königl A., 1981, ApJ, 243, 700

Lasota J.-P., 2001, New Astron. Rev., 45, 449

Magdziarz P., Zdziarski A. A., 1995, MNRAS, 273, 837

Malzac J., Belmont R., 2009, MNRAS, 392, 570

Miller J. M. et al., 2003, MNRAS, 338, 7

Narayan R., Mahadevan R., Quataert E., 1998, in Abramowicz M. A., Bjornsson G., Pringle J. E., eds, Theory of Black Hole Accretion Disks. Cambridge Univ. Press, Cambridge, p. 148

O'Donnell J. E., 1994, ApJ, 422, 158

Orosz J. A., Steiner J. F., McClintock J. E., Torres M. A. P., Remillard R. A., Bailyn C. D., Miller J. M., 2011, ApJ, 730, 75

Poutanen J., Coppi P. S., 1998, Phys. Scr., T77, 57

Poutanen J., Svensson R., 1996, ApJ, 470, 249

Poutanen J., Veledina A., 2014, Space Sci. Rev., 183, 61

Poutanen J., Vurm I., 2009, ApJ, 690, L97

Predehl P., Schmitt J. H. M. M., 1995, A&A, 293, 889

Revnivtsev M., Sazonov S., Gilfanov M., Churazov E., Sunyaev R., 2006, A&A, 452, 169

Russell D. M., Maitra D., Dunn R. J. H., Markoff S., 2010, MNRAS, 405, 1759

Russell D. M., Maitra D., Dunn R. J. H., Fender R. P., 2011, MNRAS, 416, 2311

Sánchez-Fernández C. et al., 1999, A&A, 348, L9

Shadmehri M., Khajenabi F., 2005, MNRAS, 361, 719

Shakura N. I., Sunyaev R. A., 1973, A&A, 24, 337

Suleimanov V., Meyer F., Meyer-Hofmeister E., 1999, A&A, 350, 63

Tomsick J. A., Corbel S., Kaaret P., 2001, ApJ, 563, 229

van Paradijs J., McClintock J. E., 1995, in Lewin W. H. G., van Paradijs J., van den Heuvel E. P. J., eds, Cambridge Astrophysics Series 26: X-ray binaries. Cambridge Univ. Press, Cambridge, p. 58

Veledina A., Vurm I., Poutanen J., 2011a, MNRAS, 414, 3330

Veledina A., Poutanen J., Vurm I., 2011b, ApJ, 737, L17

Veledina A., Poutanen J., Vurm I., 2013a, MNRAS, 430, 3196

Veledina A., Poutanen J., Ingram A., 2013b, ApJ, 778, 165

Wardziński G., Zdziarski A. A., 2000, MNRAS, 314, 183

Wardziński G., Zdziarski A. A., 2001, MNRAS, 325, 963

Warner B., 1995, Cambridge Astrophysics Series 28: Cataclysmic Variable Stars. Cambridge Univ. Press, Cambridge

Xue Y., Wu X.-B., Cui W., 2008, MNRAS, 384, 440

Yuan F., Zdziarski A. A., Xue Y., Wu X.-B., 2007, ApJ, 659, 541

Zdziarski A. A., Gierliński M., 2004, Prog. Theor. Phys. Suppl., 155, 99

This paper has been typeset from a TEX/LATEX file prepared by the author.